Inorg. Chem. **2007**, *46*, 4968–4978

1,2,3-Triazolate-Bridged Tetradecametallic Transition Metal Clusters $[M_{14}(L)_6O_6(OMe)_{18}X_6]$ ($M = Fe^{III}$, Cr^{III} and $V^{III/IV}$) and Related Compounds: Ground-State Spins Ranging from $S = 0$ to $S = 25$ and Spin-Enhanced Magnetocaloric Effect

Rachel Shaw,[†] Rebecca H. Laye,[†] Leigh F. Jones,[†] David M. Low,[†] Caytie Talbot-Eeckelaers,[†] Qiang Wei,[†] Constantinos J. Milios,[‡] Simon Teat,[§] Madeleine Helliwell,[†] James Raftery,[†] Marco Evangelisti,[£] Marco Affronte,[£,||] David Collison,*[,†] Euan K. Brechin,*[,†,‡] and Eric J. L. McInnes*[,†]

School of Chemistry, The University of Manchester, Manchester M13 9PL, U.K., Department of Chemistry, University of Edinburgh, Edinburgh EH9 3JJ, U.K., CCLRC Daresbury Laboratory, Daresbury, Cheshire WA4 4AD, U.K., National Research Center on "nanoStructures and bioSystems at Surfaces" (S^3), INFM-CNR, 41100 Modena, Italy, and Dipartimento di Fisica, Università di Modena e Reggio Emilia, 41100 Modena, Italy

Received February 19, 2007

We report the synthesis, by solvothermal methods, of the tetradecametallic cluster complexes $[M_{14}(L)_6O_6(OMe)_{18}Cl_6]$ ($M = Fe^{III}$, Cr^{III}) and $[V_{14}(L)_6O_6(OMe)_{18}Cl_{6-x}O_x]$ ($L =$ anion of 1,2,3-triazole or derivative). Crystal structure data are reported for the $\{M_{14}\}$ complexes $[Fe_{14}(C_2H_2N_3)_6O_6(OMe)_{18}Cl_6]$, $[Cr_{14}(bta)_6O_6(OMe)_{18}Cl_6]$ (btaH = benzotriazole), $[V_{14}O_6(Me_2bta)_6(OMe)_{18}Cl_{6-x}O_x]$ [Me_2btaH = 5,6-Me_2-benzotriazole; eight metal sites are V^{III}, the remainder are disordered between $\{V^{III}–Cl\}^{2+}$ and $\{V^{IV}=O\}^{2+}$] and for the distorted $[Fe^{III}_{14}O_9(OH)(OMe)_8(bta)_7(MeOH)_5(H_2O)Cl_8]$ structure that results from non-solvothermal synthetic methods, highlighting the importance of temperature regime in cluster synthesis. Magnetic studies reveal the $\{Fe_{14}\}$ complexes to have ground state electronic spins of $S \leq 25$, among the highest known, while in contrast the $\{Cr_{14}\}$ complex has an $S = 0$ ground state despite having a very similar structure and all complexes being dominated by intramolecular antiferromagnetic exchange interactions. The $\{Fe_{14}\}$ complexes undergo a magnetic phase transition to long-range ordering at relatively high temperatures for molecular species, which are governed by the steric bulk of the triazole ($T_N = 1.8$ and 3.4 K for L = bta^- and $H_2C_2N_3^-$, respectively). The huge spins of the $\{Fe_{14}\}$ complexes lead to very large magnetocaloric effects (MCE)—the largest known for any material below 10 K—which is further enhanced by spin frustration within the molecules due to the competing antiferromagnetic interactions. The largest MCE is found for $[Fe_{14}(C_2H_2N_3)_6O_6(OMe)_{18}Cl_6]$ with an isothermal magnetic entropy change $-\Delta S_m$ of 20.3 J kg^{-1} K^{-1} at 6 K for an applied magnetic field change of 0–7 T.

Introduction

As part of programs exploring (i) the solvothermal synthesis of transition metal cluster complexes[1] and (ii) the cluster chemistry of benzotriazole[2] (btaH, Scheme 1), we recently reported the synthesis and magnetic characterization of the tetradecametallic Fe^{III} cluster, $[Fe_{14}(bta)_6O_6(OMe)_{18}Cl_6]$ (**1**).[3] This molecule has a remarkably high electronic spin in its lowest lying states—although preliminary measurements had indicated an $S = 23$ ground state,[3] more accurate data later confirmed a value of $S = 25$ (at least in

* To whom correspondence should be addressed. E-mail: eric.mcinnes@manchester.ac.uk (E.J.L.M.); ebrechin@staffmail.ed.ac.uk (E.K.B.); david.collison@manchester.ac.uk (D.C.).
[†] The University of Manchester.
[‡] University of Edinburgh.
[§] CCLRC Daresbury Laboratory.
[£] National Research Center on "nanoStructures and bioSystems at Surfaces" (S^3).
[||] Università di Modena e Reggio Emilia.

(1) Laye, R. H.; McInnes, E. J. L. *Eur. J. Inorg. Chem.* **2004**, 2811.
(2) Collison, D.; McInnes, E. J. L.; Brechin, E. K. *Eur. J. Inorg. Chem.* **2006**, 2725, and references therein.
(3) Low, D. M.; Jones, L. F.; Bell, A.; Brechin, E. K.; Mallah, T.; Rivière, E.; Teat, S. J. McInnes, E. J. L. *Angew. Chem., Int. Ed.* **2003**, *42*, 3781.

10.1021/ic070320k CCC: $37.00
Published on Web 05/16/2007

Scheme 1. Structures of 1,2,3-Triazole Ligands Used in This Work

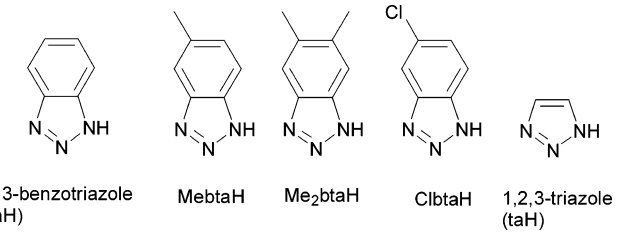

an applied magnetic field).[4] This is only surpassed by Christou's $\{Mn^{II}_6Mn^{III}_{18}Mn^{IV}\}$ cluster ($S = 51/2 \pm 1$)[5a] and Powell's $\{Mn^{III}_{12}Mn^{II}_7\}$ cluster ($S = 83/2$).[5b] Such molecules are of interest because they can display important magnetic phenomena, for instance, magnetic bistability in single molecule magnets[6] (SMMs). In SMMs a significant negative zero-field splitting (ZFS, D) splits the $2S + 1$ degeneracy of the M_S substates in zero applied magnetic field with $M_S = \pm S$ lying lowest in energy. This magnetic anisotropy provides an energy barrier of magnitude $S^2|D|$ to the reorientation of spin and, hence, blocking of the magnetization below a certain temperature which, in part, is dictated by $S^2|D|$. Despite the very large value of S, **1** does not behave as an SMM, and this is because the ZFS of the ground state is negligible (see later). However, this magnetically *isotropic* nature of its giant spin has interesting consequences, leading to an enormous magnetocaloric effect (MCE) below 10 K.[4]

The MCE is intrinsic to any paramagnet, describing temperature changes of the paramagnet on changing applied magnetic field, and is associated with the changes in magnetic entropy. Debye[7a] and Giauque[7b] proposed that the MCE could be exploited for refrigeration via adiabatic demagnetisation processes. This is illustrated by the magnetic entropy $S_m(T,H)$ curves for a paramagnet of spin S in Figure 1.[4]

A spin S has a $2S + 1$ degeneracy in zero field (neglecting ZFS), and hence, the full amount of the magnetic entropy is $R \ln(2S + 1)$, where R is the gas constant. On application of a magnetic field H this degeneracy is lifted, the spin system orders, and $S_m(T,H)$ decreases (S_m is nil on saturation of the magnetization). Thus, if a strong magnetic field H_f is applied to a paramagnet at initial temperature T_i and field H_i (say, $H_i = 0$), with the sample in thermal equilibrium with a heat bath, we isothermally magnetize the sample (A → B) with decrease in magnetic entropy ΔS_m (Figure 1). If the paramagnet is then thermally isolated and the field removed

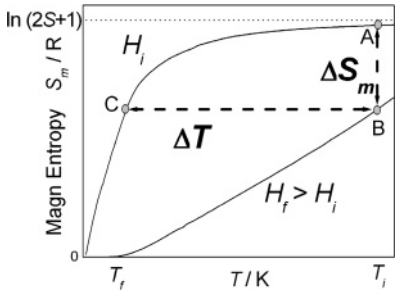

Figure 1. Magnetic entropy, S_m, as a function of temperature, T, for two different applied magnetic fields H_i and H_f where $H_i < H_f$. A → B: isothermal magnetization with entropy change ΔS_m; B → C: adiabatic demagnetization with resulting temperature change $\Delta T = T_f - T_i$.

in a reversible process we perform an adiabatic demagnetisation (B → C). Under adiabatic conditions the total entropy of the system must be constant, hence the increase in magnetic entropy ΔS_m must be compensated by a decrease in the entropy of the lattice. This results in a decrease in temperature (ΔT) of the material. High-spin ground state clusters, with potentially very large changes in S_m at low temperatures (i.e., where almost all population is in the ground state) are therefore attractive materials for low-temperature cooling[8] and in principle could be more efficient than the lanthanide and intermetallic materials conventionally used for this purpose. Tejada and co-workers have performed such measurements[9] for the archetypal SMMs $[Mn_{12}O_{12}(O_2CPh)_{16}(H_2O)_4]$ "$\{Mn_{12}\}$" and $[Fe_8O_2(OH)_{12}(tacn)_6]Br_8$ "$\{Fe_8\}$" (tacn = 1,3,5-triazacyclononane) both of which have $S = 10$ ground states. However, the significant ZFS of the ground states breaks the $2S + 1$ degeneracy in zero field, leading to blocking of the magnetization at low enough temperature. This results in a lower MCE[8] therefore limiting the potential of SMMs in this area. In contrast, the very large and isotropic ground state spin of **1** results in a huge MCE at low temperatures, with characteristic parameters of $-\Delta S_m = 17.6 \pm 2.8$ J kg^{-1} K^{-1} and $\Delta T = 5.8 \pm 0.8$ K for $T_i = 6$ K and a magnetic field change of 0−7 T, determined from variable-temperature, variable-field specific heat and magnetization measurements.[4] In other words, it should be possible to cool **1** to 6 K by conventional methods and then to achieve temperatures well below 1 K by an isothermal magnetization−adiabatic demagnetization cycle.

Given the interesting and potentially useful low-temperature physics of **1**, we set out to prepare new $[M_{14}(L)_6O_6(OMe)_{18}X_6]$ complexes, "$\{M_{14}\}$". In this work we report the extension of the solvothermal route used to prepare **1** to both different metal ions and different bridging 1,2,3-triazoles (L). We report the isolation of Fe^{III}, Cr^{III}, and $V^{III/IV}$ $\{M_{14}\}$ complexes—a very rare example where a high nuclearity cluster type can be isolated for several different metal ions, with the Cr^{III} example being the largest chromium cluster reported to date. We discuss the importance of the solvo-

(4) Evangelisti, M.; Candini, A.; Ghirri, A.; Affronte, M.; Brechin, E. K.; McInnes, E. J. L. *Appl. Phys. Lett.* **2005**, *87*, 072504. Evangelisti, M.; Candini, A.; Ghirri, A.; Affronte, M.; Piligkos, S.; Brechin, E. K.; McInnes, E. J. L. *Polyhedron* **2005**, *24*, 2573.
(5) (a) Murugesu, M.; Habrych, M.; Wernsdorfer, W.; Abboud, K. A.; Christou, G. *J. Am. Chem. Soc.* **2004**, *126*, 4766. (b) Ako, A. M.; Hewitt, I. J.; Mereacre, V.; Clérac, R.; Wernsdorfer, W.; Anson, C. E.; Powell, A. K. *Angew. Chem., Int. Ed.* **2006**, *45*, 4926.
(6) Sessoli, R.; Gatteschi, D.; Caneschi, A.; Novak, M. A. *Nature* **1993**, *365*, 141. Sessoli, R.; Tsai, H-L.; Schake, A. R.; Wang, S.; Vincent, J. B.; Folting, K.; Gatteschi, D.; Christou, G.; Hendrickson, D. N. *J. Am. Chem. Soc.* **1993**, *115*, 1804.
(7) (a) Debye, P. *Ann. Phys.* **1926**, *81*, 1154. (b) Giauque, W. F. *J. Am. Chem. Soc.* **1927**, *49*, 1864.
(8) For a recent review see: Evangelisti, M.; Luis, F.; de Jongh, L. J.; Affronte, M. *J. Mater. Chem.* **2006**, *16*, 2534.
(9) Torres, F.; Hernández, J. M.; Bohigas, X.; Tejada, J. *Appl. Phys. Lett.* **2000**, *77*, 3248; Torres, F.; Bohigas, X.; Hernández; J. M.; Tejada, J. *J. Phys.: Condens. Matter* **2003**, *15*, L119.

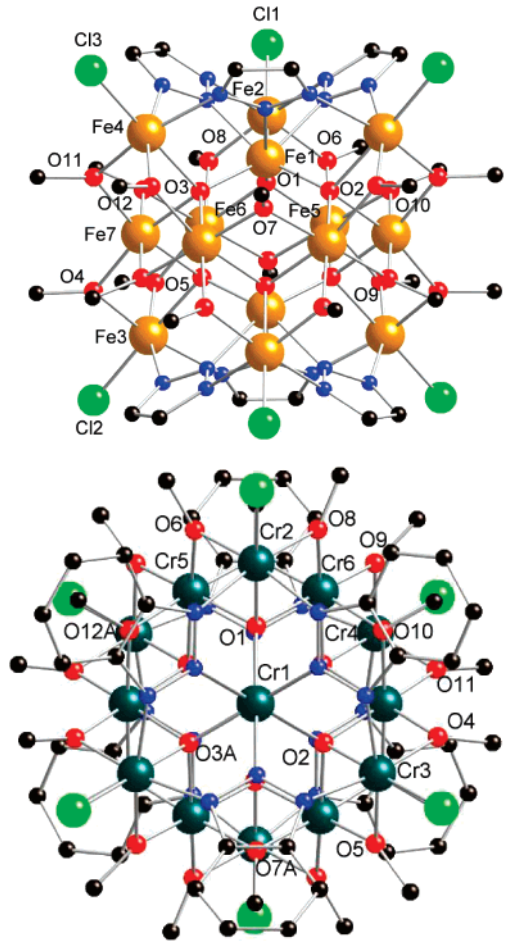

Figure 2. Molecular structures of $[Fe_{14}O_6(ta)_6(OMe)_{18}Cl_6]$ (**5**, top) and $[Cr_{14}O_6(bta)_6(OMe)_{18}Cl_6]$ (**6**, bottom), viewed approximately perpendicular to and along, respectively, the pseudo-3-fold axis (M1···M1A). The atom labeling is equivalent between the two complexes. Scheme: Fe (yellow), Cr (dark green), O (red), N (blue), C (black), Cl (light green).

thermal conditions in the synthetic chemistry of such species, giving examples of the products that form under less forcing conditions.

We report that an $S = 25$ ground or very low-lying excited state—and hence very large MCE—is general for $\{Fe_{14}\}$ with different L and hence that the triazolate has only a small influence on the intracluster magnetic exchange interactions. In contrast, when M = Cr^{III} we observe an $S = 0$ ground state rather than the $S = 15$ which would be expected to result from a similar magnetic structure to **1**. We also show that the steric bulk of the triazolate ligand, and hence of the cluster, has a strong influence on the collective behavior of the complex. Specifically, the cluster $[Fe_{14}(ta)_6O_6(OMe)_{18}Cl_6]$ (**5**), where ta is anion of 1,2,3-triazole (Scheme 1), packs significantly closer in the solid state than **1** and this results in long-range (antiferro)magnetic order at temperatures below $T_N = 3.4$ K, which is an uncommonly large ordering temperature among molecular clusters.[8] In addition, slight differences in the intramolecular couplings within this cluster cf. **1** enhance the degree of magnetic frustration that characterize the spin systems of $\{Fe_{14}\}$ complexes,[4] making available the thermal population of a

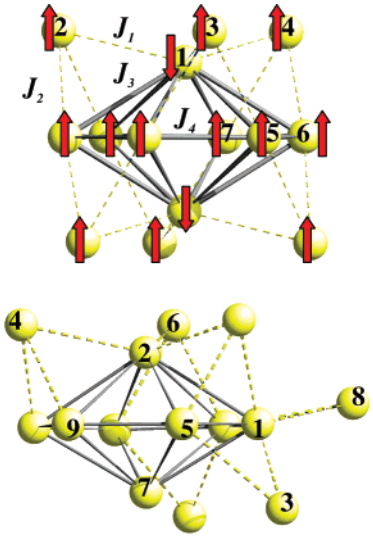

Figure 3. Comparison of metallic cores of **1** (top) and **8** (bottom), with magnetic exchange interactions and ground-state spin structure shown for **1**. Numbering of iron ions as in Figures 2 and 4.

multitude of low-energy, large spin excited states. We show that this results in a significantly larger MCE for **5** than **1**.

Results and Discussion

Synthesis and Structural Studies. (i) Analogues of 1 with Different Triazoles. We previously reported that reaction of the basic iron carboxylate $[Fe_3O(O_2CMe)_6(H_2O)_3]$-Cl with btaH in methanol at 100 °C under solvothermal conditions gives **1** as a crystalline product direct from the reaction solution in ca. 40% yield (method A, see Experimental Section).[3] Curiously, this reaction fails if oxo-centered triangles with carboxylates other than acetate are used as starting material, even though no carboxylate is found in the product. We have now found that **1** can also be prepared by a simpler reaction of $FeCl_3$, btaH, and NaOMe in MeOH, again under solvothermal conditions, albeit in reduced yield (ca. 20%, method B). Both these routes can be used to prepare analogues of **1** with different 1,2,3-triazoles. Thus, $[Fe_{14}O_6(L)_6(OMe)_{18}Cl_6]$ with L = 5-methylbenzotriazole (MebtaH; complex **2**), 5,6-dimethylbenzotriazole (Me_2btaH; **3**), and 5-chlorobenzotriazole (ClbtaH; **4**) can be prepared. These all have very similar molecular structures and magnetic properties to **1** itself and only differ significantly in their solubilities and are not discussed further here. (X-ray diffraction data are only of sufficient quality to define the connectivities of **2**−**4**, and hence their molecular formulas. Unit cell details are given in the Experimental Section for completeness.)

More significantly (see later), we can greatly reduce the steric bulk of the cluster by using 1,2,3-triazole ($C_2H_2N_3H$; taH, Scheme 1). $[Fe_{14}O_6(ta)_6(OMe)_{18}Cl_6]$ (**5**; Figure 2) is prepared from the oxo-centered triangle precursor, as in method A for **1**, again crystallizing direct from the reaction solution in ca. 20% yield on slow cooling of the superheated solution. **5** crystallizes in the $P2_1/n$ space group as **5**·4.5MeOH (Table 1), and the $\{Fe_{14}\}$ molecules have crystallographic C_i symmetry.

Table 1. Unit Cell Details for **5**, **6**, **7**, and **8**

	5·4.5MeOH	**6**·2CH_2Cl_2.4MeOH	**7**·1.3MeOH	**8**·MeOH
chemical formula	$C_{34}H_{83}Cl_6Fe_{14}N_{18}O_{28.5}$	$C_{60}H_{94}Cl_{10}Cr_{14}N_{18}O_{28}$	$C_{67.30}H_{107.2}Cl_{2.10}N_{18}O_{29.20}V_{14}$	$C_{56}H_{58}Cl_8Fe_{14}N_{21}O_{25}$
molecular weight	2194.78	5196.06	2423.32	2490.73
crystal dimens/mm^3	0.10 × 0.05 × 0.01	0.26 × 0.19 × 0.12	0.10 × 0.08 × 0.04	0.20 × 0.10 × 0.03
cryst syst	monoclinic	orthorhombic	triclinic	orthorhombic
space group	*P*2(1)/*n*	*Pbca*	$P\bar{1}$	*Pnma*
a/Å	13.049(2)	18.0588(5)	13.300(2)	21.848(2)
b/Å	17.069(3)	19.8587(6)	14.938(2)	24.513(2)
c/Å	16.566(3)	25.4792(8)	15.264(2)	17.335(1)
α/°	90	90	66.155(2)	90
β/°	108.139(2)	90	75.976(2)	90
γ/°	90	90	76.399(2)	90
U/Å^3	3506.4(10)	9137.5(5)	2658.7(6)	9283.9(13)
Z	2	2	1	4
ρ_{calcd}	2.079	1.889	1.514	1.782
T/K	150	100(2)	150	293
$2\theta_{max}$/deg	48.44	52.76	59.3	52.74
data collected	18 509	66 844	26 114	52 653
(unique)	(18 509)	(9335)	(14 135)	(9723)
data used [$I > 2\sigma(I)$]	13 220	6480	11 021	4034
no. of params	464	628	630	534
R1(*F*)	0.0492	0.0542	0.0579	0.0730
wR2	0.1188	0.1456	0.1945	0.2084
$\Delta\rho_{min}$/eÅ^{-3}	−0.688	−1.442	−0.485	−1.608
$\Delta\rho_{max}$/eÅ^{-3}	0.750	1.251	0.180	0.173

The core structure is identical to that of **1**, being based on a hexa-capped hexagonal bipyramid of Fe^{III} with the caps on alternate faces (Figures 2 and 3), with idealized D_{3d} symmetry (3-fold axis down the Fe1−Fe1A vector). Fe1 and Fe1A define the apexes of the hexagonal bipyramid, Fe5−7 and symmetry equivalents (s.e.) define the equatorial plane, and Fe2−4 and s.e. are the face-caps (Figure 3). The three face-capping iron ions and the apical iron on either half of the molecule form two $\{Fe_4(ta)_3Cl_3\}$ units, bound by μ_3-ta^- with the central two nitrogens coordinated to Fe1 (or s.e.), each separated by nine μ_2-methoxides and three μ_4-oxides [O1−3] from the central $\{Fe_6\}$ ring. The face caps each have a terminal chloride, while the coordination sphere of the apical Fe1 is completed by the (μ_4-)O1−3 which bridge it to each of Fe2−4 and to the central $\{Fe_6\}$ ring. The $\{Fe_6\}$ ring is near planar with each Fe ion bound to two μ_4-oxides bridging to Fe1 and its s.e., two μ_2-methoxides bridging to two face-capping Fe ions, and two μ_2-methoxides bridging within the $\{Fe_6\}$ ring.

(ii) Analogues of 1 with Different Metal Ions. Attempts to prepare the chromium(III) analogue of **1** via reaction of $[Cr_3O(O_2CMe)_6(H_2O)_3]Cl$ with btaH in MeOH under solvothermal conditions, in strict analogy to method A for **1**, failed. These reactions gave the decametallic wheels $[Cr_{10}(OMe)_{20}(O_2CMe)_{10}]$ that also result from this reaction in the absence of btaH, and that we have reported previously.[11] However, following method B for **1**—reaction of $CrCl_3$ with btaH and NaOMe in MeOH at 150 °C—does give the desired product $[Cr_{14}O_6(bta)_6(OMe)_{18}Cl_6]$ (**6**), albeit in low yield (ca. 5%) and only after slow evaporation of the solution that results from the initial solvothermal reaction. We reasoned that the lower yield of **6** cf. **1** may be due to the greater kinetic inertness of the Cr^{III} ion. However, higher temperatures (up to 200 °C) do not improve the yield. As an alternative route we attempted a similar reaction but using a Cr^{II} starting material, $CrCl_2$, which we reasoned would react quicker and would oxidize to the desired product. This method proved successful, giving crystalline **6** in ca. 30% crude yield direct from the reaction solution on cooling. Single crystals separated manually from the reaction byproducts were of sufficient quality for X-ray diffraction analysis. These were in the $P2_1/n$ space group (see Experimental Section). However, in order to separate **6** from insoluble byproducts, and therefore to isolate it in sufficient quantities for magnetic studies, it was necessary to recrystallize from CH_2Cl_2/MeOH. **6** crystallized in the orthorhombic space group *Pbca* as **6**·2CH_2Cl_2·4MeOH. The $\{Cr_{14}\}$ molecules have crystallographically imposed C_i symmetry, and the connectivity is identical to that in **1** (Figure 2). Selected structural parameters are in Tables 2 and 3 where we have used analogous atom labeling to **1**. **6** is the highest nuclearity Cr^{III} species isolated to date, the next largest being dodecametallic.[12]

There are very few high-nuclearity vanadium(III), or even mixed-valence vanadium(III/IV), clusters in the literature due to the easily oxidizable nature of this ion.[10,13] Therefore, the vanadium analogue of **1** was an attractive target given that we had already shown that this chemistry was common to both iron(III) and chromium(III). As with the chromium(III) chemistry, attempted synthesis of $[V_{14}O_6(bta)_6(OMe)_{18}Cl_6]$ from oxo-centered vanadium triangles failed, but

(10) Laye, R. H.; Wei, Q.; Mason, P. V.; Shanmugan, M.; Teat, S. J.; Brechin, E. K.; Collison, D.; McInnes, E. J. L. *J. Am. Chem. Soc.* **2006**, *86*, 9020.

(11) McInnes, E. J. L.; Anson, C.; Powell, A. K.; Thomson, A. J.; Poussereau, S.; Sessoli, R. *Chem. Commun.*, **2001**, 89. Low, D. M.; Rajaraman, G.; Helliwell, M.; Timko, G.; van Slageren, J.; Sessoli, R.; Ochsenbein, S. T.; Bircher, R.; Dobe, C.; Waldmann, O.; Güdel, H-U.; Adams, M. A.; Ruiz, E.; Alvarez, S.; McInnes, E. J. L. *Chem. Eur. J.* **2006**, *12*, 1385.

(12) Batsanov, A. S.; Timko, G. A.; Strutchkov, Y. T.; Gérbéléu, N. V.; Indrichan, K. M. *Koord. Khim.* **1991**, *17*, 662. Mabbs, F. E.; McInnes, E. J. L.; Murrie, M.; Parsons, S.; Smith, G. M.; Wilson, C. C.; Winpenny, R. E. P. *Chem. Commun*. **1999**, 643. Parsons, S.; Smith, A. A.; Winpenny, R. E. P. *Chem. Commun.* **2000**, 579.

Table 2. Ranges of Selected Bond Distances (Å) in **1**, **5**, **6**, and **7**

	1	5	6	7
M-μ_4O	1.952(7)−2.152(8)	1.957(3)−2.127(2)	1.970(4)−2.036(4)	1.950(2)−2.177(2)
M-μ_2O(Me)	1.959(10)−2.077(10)	1.971(3)−2.016(3)	1.951(4)−2.004(4)	1.938(2)−2.022(2)
M−N	2.114(13)−2.194(10)	2.142(3)−2.160(3)	2.038(5)−2.081(6)	2.103(3)−2.129(3)
M−Cl	2.254(5)−2.270(4)	2.257(1)−2.278(1)	2.278(2)−2.282(2)	2.115(7)−2.256(2)
V=O	n.a.	n.a.	n.a.	1.625(4)−1.676(6)

Table 3. Selected Interbond Angles (deg) in **1**, **5**, **6**, and **7**

	1	5	6	7
M1−O1−M2	113.3(4)	114.30(11)	110.49(17)	112.28(10)
M1−O1−M5	124.6(3)	124.71(12)	126.1(2)	124.67(10)
M1−O1−M6	125.9(4)	124.86(12)	125.6(2)	125.02(10)
M2−O1−M5	95.3(3)	95.76(10)	96.68(17)	96.84(8)
M2−O1−M6	96.2(3)	95.65(9)	97.19(17)	96.56(8)
M5−O1−M6	94.5(3)	94.60(10)	94.20(15)	95.03(9)
M1−O2−M3	113.1(4)	113.61(12)	110.56(17)	112.18(10)
M1−O2−M5	125.3(4)	124.68(12)[a]	125.99(19)	125.00(11)
M1−O2−M7	125.0(4)	124.45(23)	125.78(19)	124.46(10)
M3−O2−M5	96.0(3)	96.01(10)[a]	96.66(16)	96.97(8)
M3−O2−M7	96.0(3)	96.16(10)	96.48(15)	96.66(9)
M5−O2−M7	94.6(3)	95.26(10)[a]	94.52(16)	95.21(9)
M1−O3−M4	114.1(3)	113.41(12)	110.68(16)	112.39(9)
M1−O3−M6	123.7(3)	125.08(12)[b]	125.77(19)	125.44(10)
M1−O3−M7	124.7(4)	124.11(13)	126.01(19)	124.32(10)
M4−O3−M6	96.5(3)	95.68(10)[b]	96.67(16)	96.54(8)
M4−O3−M7	96.1(3)	96.09(9)	96.91(16)	96.17(9)
M6−O3−M7	95.3(3)	95.71(10)[b]	94.06(15)	95.35(8)
M3−O4−M7	100.6(4)	102.20(11)	99.8(2)	102.56(11)
M3−O5−M5	101.7(4)	102.86(12)[a]	98.6(2)	102.81(11)
M2−O6−M5	101.2(4)	102.27(12)	98.2(2)	104.05(10)
M5−O7−M6	101.0(4)	100.44(11)	98.82(17)	101.34(10)
M2−O8−M6	98.6(4)	102.20(11)	98.4(3)	103.81(10)
M4−O9−M6	100.1(4)	102.24(12)[b]	97.69(19)	102.34(11)
M6−O10−M7	101.3(4)	101.48(12)[b]	98.49(18)	101.16(9)
M4−O11−M7	100.8(3)	102.13(11)	99.00(19)	101.75(11)
M5−O12−M7	100.4(3)	101.28(11)[a]	98.4(2)	101.30(10)

[a] Fe6 not Fe5. [b] Fe5 not Fe6.

reactions starting from metallic chloride were (partially) successful. Reaction of VCl_3 with NaOMe and btaH in MeOH at 150 °C gives crystals of $[V_{14}O_6(bta)_6(OMe)_{18}Cl_{6-x}O_x]$. However, we found that better quality single crystals could be obtained using Me_2btaH in place of btaH.

$[V_{14}O_6(Me_2bta)_6(OMe)_{18}Cl_{6-x}O_x]$ (**7**) crystallizes in $P\bar{1}$ as **7**·1.3MeOH (Table 1), with the $\{V_{14}\}$ molecules lying on an inversion center. The connectivity in **7** is analogous to that in **1** (Tables 2 and 3), with one major exception. Analysis of the X-ray diffraction data shows two peaks corresponding to terminal ligands at each of the face-capping vanadium ions (V2−4 and s.e.). One of these is at 1.625(4)−1.676(6) Å from the vanadium ions while the other is at 2.115(7)−2.256(2) Å. The latter are consistent with the expected V^{III}−Cl bonds, and these peaks refine well as chlorine. However, the former distance is characteristic of the oxo-vanadium-(IV) ion and these peaks resolve well as oxygen. Hence, it appears that there has been partial oxidation of the desired product $[V_{14}O_6(Me_2bta)_6(OMe)_{18}Cl_6]$ to give **7**, which can be written alternatively as $[V^{III}_6(V^{III}Cl)_{6-x}(V^{IV}O)_xO_6(Me_2bta)_6(OMe)_{18}]$. Microanalytical data (C/H/N/V) are consistent with $x = 2$, while refinement of the X-ray data with partial occupancy gives $x = 4$. These are likely to be average parameters and in practice the solid state probably consists of a solid solution of $x = 0-6$. That these can cocrystallize is due to the isoelectronic nature of the $\{V^{III}Cl\}^{2+}$ and $\{V^{IV}O\}^{2+}$ fragments. We have as yet been unable to isolate the pure $x = 6$ or 0 complexes. Nevertheless, **7** is an example of an unusually highly reduced vanadium cluster.

Table 2 gives ranges of bond lengths involving the metal ions in **1**, **5**, **6**, and **7**, and Table 3 lists equivalent M−O−M angles.

(iii) Importance of Solvothermal Conditions in the Preparative Chemistry of $\{M_{14}\}$ Clusters. All of the $\{M_{14}\}$ clusters, **1**−**6**, above were prepared under solvothermal conditions, i.e., in sealed reaction vessels allowing high-temperature reactions and under favorable conditions for crystallization of products direct from the reaction solution.[1,14] We have explored the importance of the temperature regime in this chemistry by attempting analogous reactions under "conventional" conditions, i.e., reactions limited in temperature by the boiling point of the solvent at atmospheric pressure.

Reactions following method A for compound **1**, but under ambient or reflux conditions, resulted in dark solutions from which we failed to crystallize any product. In contrast, following method B but at room-temperature we isolated $[Fe_{14}O_9(OH)(OMe)_8(bta)_7(MeOH)_5(H_2O)Cl_8]$ (**8**) by slow evaporation of the reaction solution. **8** can also be isolated in slightly improved yields by reaction of the monometallic iron(III) species $[FeCl_3(btaH)_2]$[15] with NaOMe in MeOH at room temperature.

8 crystallizes as **8**·MeOH in the *Pnma* space group (Table 1), and the molecule lies across a mirror plane through Fe2, Fe4, Fe7, and Fe8 (C_s point symmetry, Figure 4). The metallic core has some close similarities to that of **1**, also being based on a hexacapped hexagonal bipyramid of Fe^{III} with Fe2 and Fe7 at the apexes and Fe1, Fe5, Fe9, and s.e. forming the central, near-planar $\{Fe_6\}$ ring. However, in contrast to **1**, there are only three face-caps (Fe4,6,6A) and there are now three Fe^{III} ions (Fe3,3A,8) capping *edges* of the central $\{Fe_6\}$ ring (Figure 3). The "upper half" of the molecule (as shown in Figures 3 and 4) is identical in connectivity to **1**, with the same $\{Fe_4(\mu_3\text{-bta})_3Cl_3\}$ fragment (Fe2,4,6,6A) bridged by μ_4-O (O8,9,9A) and μ_2-OMe (O1,-1A,3,4) to the central $\{Fe_6\}$ ring. The "lower half" differs greatly: the apical Fe7 is five-coordinate trigonal bipyramidal

(13) Kumagai, H.; Kitagawa, S. *Chem. Lett*. **1996**, 471. Laye, R. H.; Murrie, M.; Ochsenbein, S.; Bell, A. R.; Teat, S. J.; Raftery, J.; Güdel, H. U.; McInnes, E. J. L. *Chem. Eur. J* **2003**, *9*, 6215. Laye, R. H.; Larsen, F. K.; Overgaard, J.; Muryn, C. A.; McInnes, E. J. L.; Rentschler, E.; Sanchez, V.; Teat, S. J.; Güdel, H. U.; Waldmann, O.; Timco, G. A.; Winpenny, R. E. P. *Chem. Commun*. **2005**, 1125. Tidmarsh, I. S.; Laye, R. H.; Brearley, P. R.; Shanmugan, M.; Sañudo, E. C.; Sorace, L.; Caneschi, A.; McInnes, E. J. L. *Chem*. *Commun.* **2006**, 2560.

(14) Rabenau, A. *Angew. Chem., Int. Ed.* **1985**, *24*, 1026.

(15) Jones, L. F. Ph.D. Thesis, The University of Manchester, 2003.

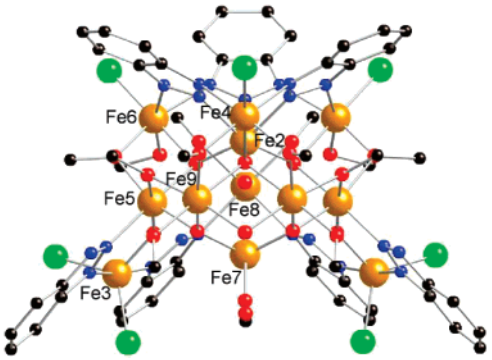

Figure 4. Molecular structure of $[Fe_{14}O_9(OH)(OMe)_8(bta)_7(MeOH)_5(H_2O)Cl_8]$ (**8**) viewed parallel to the mirror plane containing Fe2, 4, 7, and 8.

and is bridged directly only to the $\{Fe_6\}$ ring, via three μ_3-oxides (O10,15,15A), with its remaining ligands being terminal MeOH (O13) and water (O18). In place of face-caps there are three edge-capping irons—these fall into two types. Fe3 (and s.e.) is five-coordinate and caps the Fe1···Fe5 (and s.e.) edge of the $\{Fe_6\}$ ring via μ_3-oxide (O7 and s.e.); a μ_3-bta$^-$ binds Fe3 to Fe1 and to Fe8 (see below), while a μ_2-bta$^-$ 1,2-bridges to Fe5. Fe3 (and s.e.) also has two terminal chlorides and its geometry is trigonal bipyramidal with N−Fe−N defining the axial direction. Fe3 and Fe3A lie significantly below the plane of the $\{Fe_6\}$ ring. The second type of edge-cap, Fe8, lies approximately in this plane, capping the Fe1···Fe1A edge via O12. Fe8 is bound by two μ_3-bta$^-$, bridging to Fe3 and s.e., and has two terminal methanols and a terminal chloride trans to O12. The bridging within the central $\{Fe_6\}$ ring is via μ_3- and μ_4-O^{2-} (O10,15 and O8,9 respectively), μ_2-OMe^- (O5,5A) and a single μ_2-OH^- (O14). The oxidation state of all the metal ions is Fe^{III}, as assigned by bond valence sum calculations,[16] which also support the formulation of the bridging oxides and hydroxides. Selected metric parameters for **8** are in Table S1 (see Supporting Information).

We reported recently that a similar non-solvothermal reaction with vanadium(III) starting materials [VCl_3 with Me_2btaH and NaOMe in MeOH at room temperature] gives the mixed-valence $V^{III/IV}$ species $[(V^{IV}O)_8V^{III}_2(Me_2bta)_8(OH)_4(OMe)_{10}]$ (**9**).[10] **9** consists of a square-prism of vanadyl ions bridged to an internal $V^{III}_2(OMe)_2$ dimer. The edges of the square faces are formed via the 1,3-bridging mode of the triazolates; four of these are μ_2 and four are μ_3. The analogous complex with btaH, rather than Me_2btaH, can also be prepared, although the crystal structure is considerably more disordered.

The differences between the structures of **8** and **9** cf. the $\{M_{14}\}$ structures **1** and **7** highlight two important features of the solvothermal conditions used to prepare **1** and **7**. Both **8** and **9** contain a mixture of μ_2- and μ_3-triazoles, whereas the species formed under solvothermal conditions contain only the maximal μ_3 coordination mode. We have previously noted the tendency of solvothermal conditions to force the maximal coordination modes of bridging ligands, e.g., with

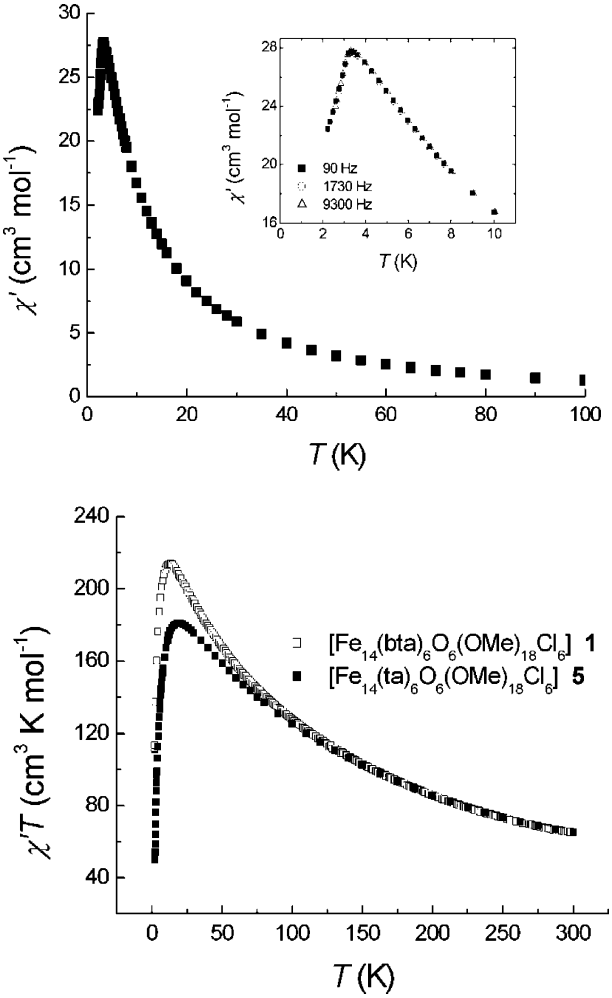

Figure 5. Plots of the ac magnetic susceptibility (χ') vs temperature (top) and $\chi'T$ vs T (bottom) for **5** measured in an ac magnetic field of 10 G and for frequencies 90, 1730, and 9300 Hz, as labeled. Inset (top): expanded χ' vs T data for **5** at 2−10 K. $\chi'T$ vs T data for **1** (□) are included in the bottom graph for comparison.

tripodal alcohols,[17] resulting in high nuclearity and high-symmetry clusters. The lower coordination modes result in less compact (with respect to metal ions) and less-symmetric structures. Thus, **8** has C_s symmetry and contains three edge-capping Fe^{III} ions (capping the hexagonal bipyramid), compared to the idealized D_{3d} symmetry of **1** with only *face*-capping metal ions (Figure 3). Similarly in the vanadium chemistry, compound **9** has only 2-fold symmetry and is much more open than **7**. These two compounds also highlight a second important feature of the solvothermal conditions: under conventional conditions we obtain a product with a V^{III}/V^{IV} ratio of 2:8, while solvothermal conditions give a 12:2 (on average) product. Here the alcohol solvent is more reducing under solvothermal conditions, thus allowing isolation of less oxidized products. These contrasts between **1** and **8** and **7** and **9** highlight the importance of exploring a wide temperature range in cluster chemistry.

Magnetic Studies. The room-temperature $\chi'T$ value of **5** is 61 cm^3 K mol^{-1} (χ' = molar magnetic susceptibility),

(16) Brown, I. D.; Altermatt, D. *Acta Crystallogr., Sect. B* **1985**, *41*, 244.

(17) Shaw, R.; Tidmarsh, I. S.; Laye, R. H.; Breeze, B.; Helliwell, M.; Brechin, E. K.; Heath, S. L.; Murrie, M.; Ochsenbein, S.; Güdel, H. U.; McInnes, E. J. L. *Chem. Commun.* **2004**, 1418.

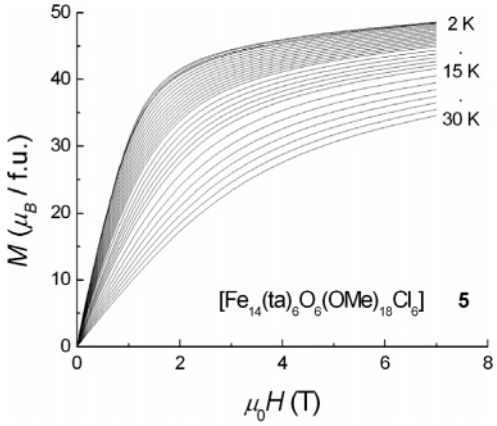

Figure 6. Experimental magnetization vs applied magnetic field for **5** at several temperatures.

consistent with 14 high-spin Fe^{III} ions. On decreasing temperature, this value increases steadily reaching a maximum of 180 cm^3 K mol^{-1} at ca. 19 K (Figure 5; data for **1** are also shown for comparison), before decreasing rapidly to ca. 48 cm^3 K mol^{-1} at 2 K. The large maximum value in $\chi'T$ suggests low-lying states of very large spin.

Low-temperature magnetization measurements as a function of applied magnetic field for **5** reveal that the molar magnetization is tending toward saturation at around 50 μ_B (Figure 6), in an applied field of around 7 T at 2 K, consistent with a ground state spin of $S = 25$ in this field. A saturation magnetization of 50 μ_B has also been observed for **1**,[4] albeit at much lower applied fields (ca. 3 T at 2 K).

Thus, changing the bridging ligand from bta^- to ta^- (compound **1** to **5**) has not grossly affected the molecular magnetic properties, both molecules having either ground states or very low-lying excited states of $S = 25$. The massive value of S can be rationalized: considering the hexa-capped hexagonal bipyramidal topology of Fe^{III} (Figure 3) and only considering magnetic exchange interactions (J) between single-atom-bridged metal ions (Figure 2), there are only four chemically distinct interactions in **1** and **5**:

(i) six J_1 interactions between the apical Fe ions (Fe1 and s.e.) and the face-capping ions (Fe2−4 and s.e.). These ions are bridged via μ_4-oxide with Fe−O−Fe angles in the range 113.41(12)−114.30(11)°,

(ii) 12 J_2 interactions between the face-capping ions (Fe2−4 and s.e.) and those in the central {Fe_6} ring (Fe5−7 and s.e.), via μ_2-OMe [102.13(11)−102.86(12)°] and μ_4-oxide [95.65(9)−96.16(10)°],

(iii) 12 J_3 interactions between the apical ions (Fe1 and s.e.) and those in the {Fe_6} ring (Fe5−7 and s.e.), via μ_4-oxide [124.11(13)−125.08(12)°], and

(iv) six J_4 interactions between adjacent ions in the central {Fe_6} ring, via μ_2-OMe [100.44(11)−101.48(12)°] and μ_4-oxide [94.60(10)−95.71(10)°].

Assuming that all four interactions are antiferromagnetic, then from the Fe−O−Fe bridging angles, we would expect the relative magnitudes of these interactions to be in the order $|J_3| > |J_1| > |J_2| \approx |J_4|$, with the first two significantly larger than the second two. Figure 3 shows that these four antiferromagnetic interactions cannot be satisfied simultaneously and, hence, that the total spin states will be determined by the *competing* interactions, leading to frustration. For the ground state, a spin structure where the apical iron ions are, say, "spin down" with all remaining ions "spin up" will result if the J_3/J_2, J_1/J_2, and J_3/J_4 ratios are large enough to force the spins of the face-capping Fe^{III} ions and those of central {Fe_6} ring to be parallel (Figure 3). This would give $S = (12 \times 5/2) - (2 \times 5/2) = 25$. Although modeling the susceptibility data to determine J_1-J_4 by conventional methods is precluded by the size of the spin system, we have attempted to estimate them in the case of **1** via DFT calculations coupled with Monte Carlo simulations,[18] giving $J_1 = -22$ cm^{-1}, $J_2 = -9$ cm^{-1}, $J_3 = -30$ cm^{-1}, $J_4 = -4$ cm^{-1} ($\hat{H} = -J_i\hat{S}_a\cdot\hat{S}_b$) which suggest that the model above is plausible.

However, a well-isolated $S = 25$ ground state would give a low-temperature limiting χT value of 325 cm^3 K mol^{-1}, and clearly this is not achieved for **1** or **5**: the maximum in $\chi'T$ is ca. 180 and 214 cm^3 K mol^{-1} for **5** and **1**, respectively (Figure 5). Possible causes of the downturn in $\chi'T$ at low temperature are (i) ZFS of the ground state, (ii) intermolecular interactions, or (iii) population of low-lying excited states. The first explanation can be ruled out by EPR spectroscopy: Q- and W-band spectra of **1** and **5** at 4 K, as powders and as frozen solutions, show only a single broad line of peak-to-peak width ca. 4000 G—this implies that the magnitude of the ground state ZFS is negligible (<0.01 cm^{-1}) in both complexes.

Intermolecular interactions are expected to play an important role at low temperatures, given the large magnetic moment of the {Fe_{14}} complexes. In **5** these interactions are manifest in a sharp spike in χ' vs T at 3.4 K (independent of frequency when measured by ac methods, see Figure 5 top and inset), indicating the onset of long-range (antiferro)-magnetic ordering of the lattice. This transition is also observed in specific heat measurements (data not shown). We have observed a similar transition in **1**,[4] but at the lower temperature of $T_N = 1.8$ K. This ordering temperature is too high to justify on the basis of a pure dipolar interaction between $S = 25$ objects, and intermolecular superexchange interactions must be playing a role. In **1** the nearest intermolecular separations are 12.948 and 14.225 Å (centroid−centroid), while the significantly smaller steric bulk of the triazolate ligands in **5** results in equivalent distances of 12.262 and 13.049 Å (**1** and **5** pack equivalently, see Supporting Information) and we expect stronger intermolecular interactions. Hence, the closer molecular packing of **5** cf. **1** gives rise to a higher transition temperature to long-range ordering for **5**. However, the $\chi'T$ vs T curves for **1** and **5** have their maxima at ca. 13 and 19 K, respectively (Figure 5), i.e., well above the respective ordering temperatures. In addition, the value of χ' at T_N is well below that expected for $S = 25$ (Figure 5, inset). These data imply that the $S = 25$ state is not exclusively populated at T_N.

(18) Rajaraman, G.; Cano, J.; Brechin, E. K.; McInnes, E. J. L. *Chem. Commun.* **2004**, 1476.

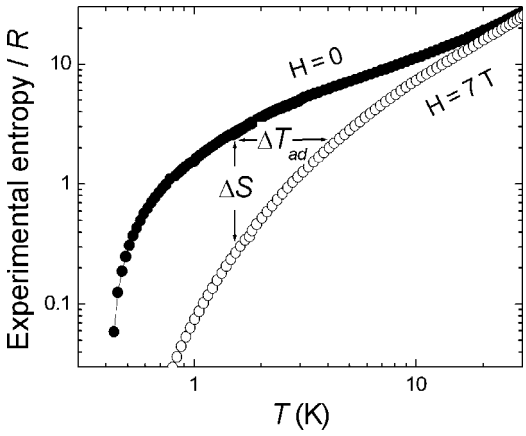

Figure 7. Entropy−temperature curves for **1** for applied magnetic fields of $H = 0$ (●) and 7 T (○), determined from variable-temperature and field-specific heat measurements (ref 4).

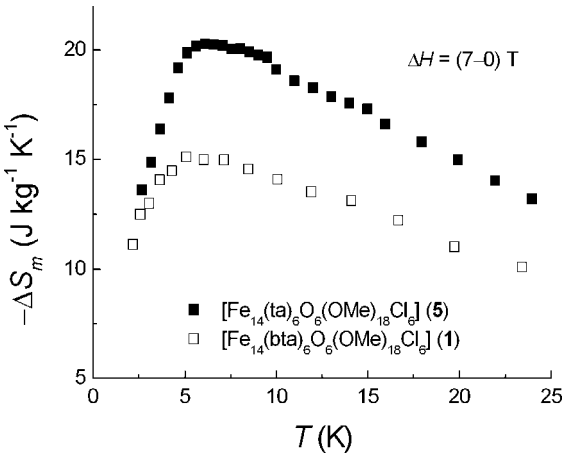

Figure 8. Magnetic entropy changes ΔS_m for **1** (□, ref 4) and **5** (■) as a function of initial temperature for an applied magnetic field change of $H = 0-7$ T, determined from the experimental magnetization data reported in ref 4 for **1**, and in Figure 6 for **5**, respectively.

Hence, we conclude that the main contribution to the low-temperature $\chi'T$ behavior of **1** and **5** has to be the presence of excited spin states at thermally accessible energies. The frustration of the intramolecular exchange interactions results in low-lying states of similar S, but lower than 25, at relative energies determined by the J_3/J_2, J_1/J_2, and J_3/J_4 ratios. These inhibit complete population of the $S = 25$ state in the small applied fields of the susceptibility experiments. The fact that the maximum value of $\chi'T$ for **5** lies well below that of **1** indicates a larger degree of frustration in the former and, hence, a greater density of low-lying spin states. This is also apparent in the higher applied fields necessary to saturate the magnetization in **5**, and it is possible that the $S = 25$ state is itself a low-lying excited state (in zero-applied field) in **5**. These subtle changes in relative energies of low-lying spin states would require only very small changes in the J_3/J_2, J_1/J_2, and J_3/J_4 ratios and hence very small differences in the metric parameters of **1** and **5** (Tables 2 and 3).

As described in the Introduction, the huge ground (or very low-lying) state S of **1** gives rise to a very large MCE because of the large magnetic entropy changes on magnetization/demagnetization. Figure 7 gives entropy-temperature curves determined for **1**, by methods described previously, for applied magnetic fields of 0 and 7 T.[4] The maximum MCE response is revealed by plotting the isothermal entropy change as a function of temperature (Figure 8), and for **1** the maximum in $-\Delta S_m$ is 15.3 J kg^{-1} K^{-1} at $T = 6$ K. This corresponds to a temperature change on adiabatic demagnetization of $\Delta T = 5.8 \pm 0.8$ K.[4] These values are higher than those for any other material for temperatures below 10 K, at least 30% larger than the alloys $(Er_{1-x}Dy_x)Al_2$ ($x > 0.5$), which are the next best materials.[20]

Magnetic phase transitions are associated with large entropy changes in a narrow temperature range around T_N, which may lead therefore to a significant MCE.[19] However, this cannot be the main reason for the very large MCE in the $\{Fe_{14}\}$ complexes because T_N is significantly below the temperature where the maximum MCE is observed. Hence, the MCE is due to the very large spin. However, the observed ΔS_m is in fact too large to be explained simply by the large value of S because the maximum possible for $S = 25$ is $|\Delta S_m| = R \ln(2S + 1) = 3.9R$, corresponding to 13.9 and 15.9 J kg^{-1} K^{-1} for **1** and **5**, respectively. The only possible source for the observed excess of magnetic entropy again lies in the large degree of internal frustration of the clusters (see above), leading to low-lying excited spin states that are thermally accessible even at these low temperatures. We therefore hoped that the larger frustration in **5**, as discussed above, would lead to an even higher MCE for this material. Figure 8 gives ΔS_m as a function of T for **1** and **5**, determined from $M(H,T)$ data (Figure 6) by methods described elsewhere.[4]

The maximum response for **5** is also at ca. 6 K, but $-\Delta S_m$ is significantly enhanced by over 30% cf. **1**, at 20.3 J kg^{-1} K^{-1}. We thus emphasize that **1** and **5** have significant potential as low-temperature magnetic refrigerants because of their huge spin lowest lying states, with **5** being better than **1** due to the higher degree of frustration. Direct MCE measurements, as well as a detailed theoretical investigation of the electronic spin configurations, of these materials are underway and will be reported later.

The magnetic behavior of the distorted $\{Fe_{14}\}$ structure **8** is very different. The room-temperature value of χT is 16.5 cm^3 K mol^{-1} and decreases almost linearly down to ca. 30 K where it plateaus at a value of around 9 cm^3 K mol^{-1} (Figure 9). This low-temperature value suggests an $S = 4$ ground state. A lower spin ground state than **1** and **5** is easy to rationalize, as there is no direct link between the "bottom" apical iron ion (Fe7) and the edge caps (Fe8,3,3A; Figure 3), hence these spins can align antiparallel with those of the central $\{Fe_6\}$ ring. However, $S = 4$ cannot be rationalized on the basis of a simple "spin up−spin down" model as for **1** and **5** and suggests that the competing antiferromagnetic

(19) Manuel, E.; Evangelisti, M.; Affronte, M.; Okubo, M.; Train C.; Verdaguer, M. *Phys. Rev. B* **2006**, *73*, 172406. Evangelisti, M.; Manuel, E.; Affronte, M.; Okubo, M.; Train, C.; Verdaguer, M. *J. Magn. Magn. Mater.* **2006**, in press.

(20) Lima, A. L.; Gschneider Jr., K. A.; Pecharsky, V. K.; Pecharsky, A. O. *Phys. Rev. B* **2003**, *68*, 134409.

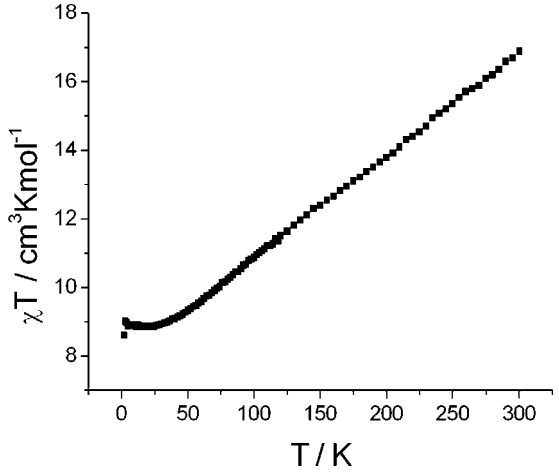

Figure 9. χT vs T for **8**, measured in applied magnetic fields of 2000 (300−50 K) and 500 G (50−2 K).

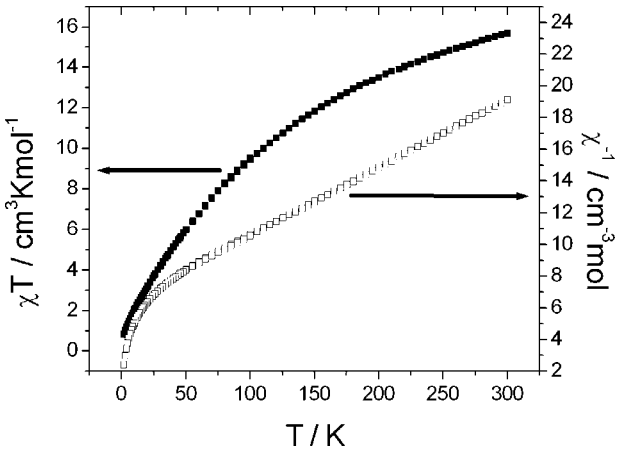

Figure 10. χT vs T for **6**, measured in applied magnetic fields of 500 (2−100 K) and 1000 G (100−300 K).

exchange interactions in **8** are similar in magnitude to each other. The complexity and low symmetry of the structure negate modeling of the susceptibility data.

The magnetic behavior of **6**, the Cr^{III} analogue of **1**, is very different again. At room temperature, χT is at a value of 15.7 cm^3 K mol^{-1} and is already decreasing rapidly with decrease in temperature (Figure 10). χ^{-1} vs T is linear between 300 K and ca. 50 K (Figure 10), and fitting to this region gives a Curie constant of 23.4 cm^3 K mol^{-1}, close to the value expected for 14 Cr^{III} ions with a g-value less than 2. At low temperatures, χT is tending toward zero, indicating a diamagnetic ground state. Thus, the competing antiferromagnetic interactions that result in the $S \leq 25$ ground state of **1** and **5** lead to an $S = 0$ state in **6** and not the $S = 15$ state that would result from a similar spin structure. This implies that the J_3/J_2, J_1/J_2, and J_3/J_4 ratios must be much smaller in **6**, such that the competing antiferromagnetic interactions lead to a very low (or zero) net spin in the ground state. Unfortunately, this frustration[21] precludes the use of Quantum Monte Carlo methods for modeling the susceptibility data. The very different magnetic behavior may have its roots in the different M−O−M angles in **6** cf. **1** (or **5**). In the Cr complex **6**, the angles corresponding to the J_1 interactions (via oxide, O1−3) and J_2 and J_3 interactions (via alkoxide, O4−8,9−12) are significantly smaller (by a few deg) than in the Fe_{14} analogues. However, predicting the effect of these changes on the magnetic structure is not straightforward.

The magnetic properties of **7** were not measured given the likely solid solution nature of $[V_6(VCl)_{6-x}(VO)_x(Me_2bta)_6(OMe)_{18}]$ in the solid state.

Conclusions

In summary, we have developed a general synthetic route to the $\{M_{14}\}$ structural type for M = Fe, Cr, and V. We have illustrated the importance of the solvothermal heating regime on the compactness of the resulting molecular structures (by forcing the maximum, μ_3-coordination modes of the 1,2,3-triazolates) and on the level of oxidation of the cluster when M is redox active (V). We have shown that the M = Cr and Fe clusters have remarkably different magnetic behaviors, with $S = 0$ and $S \leq 25$ ground state electronic spins, respectively, despite both being dominated by intramolecular antiferromagnetic interactions. Within the series of Fe complexes we observe major differences in the intermolecular interactions leading to long-range magnetic ordering at temperatures governed by the steric bulk of the triazolates. We also observe a more subtle intramolecular effect where very small changes in the exchange couplings lead to small changes in the relative energies, and density, of the low lying spin states. This latter phenomenon enhances the magnetic entropy available at low temperatures, already very large due to the huge spins involved, and consequently to an enhanced MCE (as judged by the isothermal magnetic entropy changes). For this reason **5** has an even larger MCE (by ca. 30%) than **1**. Hence, this work not only further illustrates that very large MCEs can be derived from molecular cluster species but also that it can be tuned by simple chemical modifications. The MCE found for these materials are by far the largest reported to date in the temperature regime below 10 K, and hence, these materials are of potential interest in low-temperature cooling applications.

Experimental Section

Materials and Procedures. All chemicals were purchased from Aldrich and were used without further purifications. Solvents were purchased from BDH; methanol was distilled using standard techniques for anaerobic synthetic procedures. Manipulations of $CrCl_2$ were performed in a dinitrogen-purged glove box, and for the synthesis of **7**, all manipulations were conducted under anaerobic conditions.

Physical Measurements. Crystallography. Crystal data, data collection, and refinement parameters for **1**, **5**, **6**, **7**, and **8** are in Table 1, and selected bond lengths and angles are Tables 2 and 3. Single-crystal X-ray diffraction data were collected on a Bruker Smart APEX CCD area detector using Mo Kα radiation (λ = 0.71073 Å) and ω scans (**2**, **8**), an Oxford Diffraction XCalibur2 area detector using Mo Kα radiation (λ = 0.71073 Å) and ω scans (**3**, **4**, **6**), or a Bruker Smart APEX CCD area detector using synchrotron radiation (λ = 0.68930 Å) and ω scans at Daresbury

(21) The term "frustration" strictly only applies in the case of a degenerate ground state, see Kahn, O. *Chem. Phys. Lett.* **1997**, *265*, 109.

Laboratories station 9.8 (**5**, **7**). All diffractometers were equipped with an Oxford Cryosystems low-temperature device. Data were corrected for Lorentz and polarization factors. Absorption corrections were applied to all data. All structures were solved by direct methods using SHELXS-97. All structures were completed by iterative cycles of Δ*F*-syntheses and full-matrix least-squares refinement. All refinements were against F^2 and used SHELX-97.[22]

Data for **2**−**4** were of insufficient quality to allow full structure analysis but were suitable for the structures to be confirmed as $[Fe_{14}O_6(L)_6(OMe)_{18}Cl_6]$ (unit cell details given below). The crystals of **5** were found to be twinned, and a twin correction had to be applied (see cif for full details). For **7**, all atoms were refined anistropically except for the partially occupied and disordered solvent molecules. The hydrogens on the methyl groups of the Me_2-bta ligands were found, and these were refined using a riding model. H-atoms on the methoxides and solvent molecules could not be found and were omitted from the refinement. For all other molecules, all non-H atoms were refined anisotropically, except those of any partially occupied solvent molecules, and H atoms were included in calculated positions except those of any solvent molecules which were not included.

Magnetic Measurements. For complexes **1** and **5**, magnetic moment and susceptibility data down to 2 K and for the $0 < H < 7$ T magnetic field range, were obtained with commercial Quantum Design magnetometers with an ac option. Magnetic data for **6** and **8** were measured by dc methods, in applied fields of 500 (below 100 K) and 1000 G—there was no significant dependence of the low-temperature data with applied field. All data were collected on powdered samples of the compounds.

Synthesis. $[Fe_{14}O_6(bta)_6(OMe)_{18}Cl_6]$ (1). Method A.[3] A solution of $[Fe_3O(O_2CMe)_6(H_2O)_3]Cl$ (0.30 g, 0.48 mmol) and btaH (0.17 g, 1.43 mmol) in methanol (9 mL) was heated in a Teflon-lined autoclave at 100 °C for 12 h under autogenous pressure. Cooling to room temperature at a rate of 0.05 °C min^{-1} gives red crystals and an orange precipitate. The insoluble precipitate was separated by repeated washing and decanting, leaving the red crystals of **1** which were air-dried (40% yield based on iron). Elemental analysis (%), observed (calculated for $Fe_{14}C_{54}H_{78}Cl_6N_{18}O_{24}$): C, 26.51 (27.40), H, 3.10 (3.33), N, 10.21 (10.69), Cl, 9.56 (9.02), Fe, 32.03 (33.16). IR (KBr) ν/cm^{-1}: 2924 (m), 2821 (m), 1574 (w), 1491 (w), 1444 (w), 1348 (w) 1274 (w), 1223 (s), 1136 (w), 1057 (s), 996 (w), 926 (w), 788 (m), 757 (s), 642 (w), 573 (s), 471 (s).

Method B. A solution of anhydrous $FeCl_3$ (0.30 g, 1.85 mmol), btaH (0.22 g, 1.85 mmol), and NaOMe (0.10 g, 1.85 mmol) in methanol (9 mL) was heated in a Teflon-lined autoclave at 100 °C min^{-1} for 12 h under autogenous pressure. Cooling to room temperature at 0.05 °C min^{-1} results in red crystals and an insoluble orange precipitate. The red crystals of **1** were isolated as above (20%). Elemental analysis, observed (calculated for $Fe_{14}C_{54}H_{78}Cl_6N_{18}O_{24}$): C, 27.00 (27.40), H, 3.12 (3.33), N, 10.33 (10.69). IR (KBr) ν/cm^{-1}: 2923 (m), 2820 (m), 1572 (w), 1489 (w), 1444 (w), 1349 (w) 1272 (w), 1223 (s), 1137 (w), 1055 (s), 998 (w), 926 (w), 788 (m), 755 (s), 641 (w), 574 (s), 470 (s).

$[Fe_{14}O_6(L)_6(OMe)_{18}Cl_6]$ [L = Me_2bta^- (2), $Mebta^-$ (3), $Clbta^-$ (4)]. Similar reactions as for **1**, but substituting L (0.48 mmol) for btaH, yield **2**−**4** in 20−40% yield. **2**: Elemental analysis, observed (calculated): C 30.20 (31.38), H 3.62 (4.07), N 9.68 (9.98), Cl 9.01 (8.42), Fe 30.40 (30.95). IR (KBr) ν/cm^{-1}: 2926 (m), 2821 (m), 1566 (m), 1487 (m), 1458 (m), 1437 (m), 1284 (w), 1285 (w), 1222 (m), 1172 (w), 1058 (s), 1000 (m), 854 (m) 824 (w), 699 (w), 572 (m), 467 (m). Unit cell details: triclinic $P\bar{1}$, a = 15.003(2) Å, b = 16.881(2) Å, c = 23.393(3) Å, α = 95.627(2)°, β = 91.418(2), γ = 106.937(2)°, V = 5390.8(12) $Å^3$, Z = 2. **3**: Elemental analysis, observed (calculated for $Fe_{14}C_{60}H_{90}Cl_6N_{18}O_{24}$): C, 28.59 (29.48), H, 3.61 (3.69), N, 10.51 (10.32), Cl, 9.59 (8.72), Fe, 32.49 (32.10). IR (KBr) ν/cm^{-1}: 2923 (m), 2820 (m), 1437 (w), 1269 (m), 1224 (m), 1059 (s), 835 (w), 807 (m), 765 (w), 573 (s), 473 (m). Unit cell details: monoclinic $P2(1)/n$, a = 15.6975(32) Å, b = 13.6998(31) Å, c = 20.3164(44) Å, β = 94.868(17)°, V = 4353.33 $Å^3$, Z = 2. **4**: Elemental analysis, observed (calculated for $Fe_{14}C_{54}H_{72}Cl_{12}N_{18}O_{24}$): C, 24.13 (25.29), H, 2.48 (2.83), N, 9.65 (9.83), Cl, 16.94 (16.59), Fe, 29.91 (30.49). IR (KBr) ν/cm^{-1}: 2926 (w), 2822 (w), 1465 (w), 1431 (w), 1276 (w), 1220 (w), 1056 (s), 941 (m), 813 (s), 723 (m), 600 (s), 473 (m). Unit cell details: triclinic $P\bar{1}$, a = 14.5095(26) Å, b = 18.3622(31) Å, c = 19.4758(28) Å, α = 83.726(13)°, β = 71.622(14)°, γ = 83.814(14)°, V = 4879.93 $Å^3$, Z = 2.

$[Fe_{14}O_6(ta)_6(OMe)_{18}Cl_6]$ (5). A similar reaction for **1** (method A), but substituting triazole ($C_2H_2N_3H$, taH) (0.09 g, 1.43 mmol) for btaH, gives **5** in 20% yield. Elemental analysis of dried (fully desolvated) sample, observed (calculated for $Fe_{14}C_{30}H_{66}Cl_6N_{18}O_{24}$): C, 17.00 (17.51), H, 2.88 (3.23), N, 12.27 (12.25), Cl, 11.11 (10.34), Fe, 37.01 (38.00). IR (KBr) ν/cm^{-1}: 2924 (w), 2819 (m), 1445 (w), 1205 (m), 1124 (m), 1060 (s), 976 (m), 808 (s), 722 (w), 575 (s), 471 (m).

$[Cr_{14}O_6(bta)_6(OMe)_{18}Cl_6]$ (6). Method 1. A solution of $CrCl_3 \cdot 6H_2O$(2.4 mmol), btaH (0.29 g, 2.4 mmol), and NaOMe (0.07 g, 1.2 mmol) in MeOH (9 mL) was heated in a Teflon-lined autoclave at 150 °C for 12 h. Slow cooling to room temperature gives a dark green solution. Slow evaporation gave green hexagonal plate-shaped crystals, together with an insoluble brown precipitate, after 6 weeks. The crystals were separated manually (ca. 5% crude yield).

Method 2. A similar reaction to method 1, but using $CrCl_2$ (0.30 g, 2.4 mmol) in place of $CrCl_3 \cdot 6H_2O$, yielded small block-shaped green crystals of **6** directly from the reaction solution, together with an insoluble brown precipitate. The crystals could be separated manually [28% crude yield; unit cell details: monoclinic $P2(1)/n$, a = 15.004(2) Å, b = 19.315(3) Å, c = 23.320(2) Å, β = 110.158(3)°, V = 3890.0(10) $Å^3$, Z = 2]. However, for an analytically pure sample, the crystals and powder were filtered, washed with methanol, dried, then dissolved in CH_2Cl_2, filtered, and layered with MeOH to obtain X-ray quality crystals (Table 1). Elemental analysis of dried sample, observed (calculated for $\mathbf{6} \cdot 3CH_2Cl_2$): C, 26.55 (26.76), H, 3.30 (3.31), Cl, 17.18(16.63), Cr, 28.05 (28.45), N, 9.76 (9.85). IR (KBr): ν/cm^{-1}: 3432 (br), 2925 (s), 2821 (w), 1629 (w), 1439 (w), 1280 (m), 1230 (m), 1067 (s), 796 (m), 759 (m), 621 (s), 538 (s), 439 (w).

$[V_{14}O_6(bta)_6(OMe)_{18}Cl_{6-x}O_x]$ (7). A similar reaction to method B for iron was performed. A mixture of VCl_3 (0.25 g, 1.59 mmol), Me_2btaH (0.46 g, 3.18 mmol), and NaOMe (0.17 g, 3.18 mmol) in methanol was heated in a Teflon-lined autoclave at 150 °C for 12 h. Slow cooling to room temperature yielded small brown block-shaped crystals of **7**, which could be separated by decanting and washing with methanol to leave the crystals which were dried under dinitrogen (15%). Elemental analysis of dried sample, observed (calculated for $C_{66}H_{102}N_{18}O_{26}Cl_4V_{14}$): C, 31.06 (32.78), H 3.93 (4.25), N 10.38 (10.42), Cl 5.99 (5.86), V 29.01 (29.49). IR (KBr) ν/cm^{-1}: 2924 (m), 2817 (m), 1445 (w), 1228 (w), 1064 (s), 968 (m), 793 (m), 755 (m), 605 (m), 495 (m).

$[Fe_{14}O_9(OH)(H_2O)(OMe)_8(bta)_7(MeOH)_5(Cl)_8]$ (8). Addition of addition of NaOMe (0.17 g, 1.25 mmol) to a solution of $FeCl_3$ (0.5 g, 1.25 mmol) and btaH (0.37 g, 1.25 mmol) in MeOH (40 cm^3) was left standing for 24 h then filtered to remove an insoluble

(22) *SHELXL-PC Package*; Bruker Analytical X-ray Systems: Madison, WI, 1998.

precipitate. Slow evaporation of the filtrate gave red platelike crystals of **8** (ca. 25%). Elemental analysis (%), observed (calculated for $C_{55}H_{75}O_{24}N_{21}Cl_8Fe_{14}$): C, 26.20 (26.61), H, 2.55 (3.02), N, 12.13 (11.85); Selected IR bands (KBr) ν/cm^{-1}: 1618 (m), 1573 (w), 1443 (m), 1272 (m), 1222 (s), 1146 (w), 1036 (m), 993 (w), 789 (s), 748 (s), 641 (m), 595 (w), 563 (w).

Acknowledgment. The authors thank S. Carretta and P. Santini for valuable discussions. We thank the Leverhulme Trust, the EPSRC, and the EC (NMP3-CT-2005-515767 "Magmanet") for funding.

Supporting Information Available: Crystallographic cif files and thermal ellipsoid plots for **5**−**8**; metric parameters for **8**; packing diagrams for **1** and **5**. This material is available free of charge via the Internet at http://pubs.acs.org.

IC070320K